G4SEE: A Geant4-Based Single Event Effect Simulation Toolkit and Its Validation Through Monoenergetic Neutron Measurements

Dávid Lucsányi, Rubén García Alía, *Member, IEEE*, Kacper Biłko, Matteo Cecchetto, Salvatore Fiore, *Member, IEEE*, and Elisa Pirovano

***Abstract*— A single-event effect (SEE) simulation toolkit has been developed at CERN for the whole radiation effects community and released as an open-source code. It has been validated by comparing the simulated energy deposition of inelastic interactions, due to monoenergetic neutrons in the 1.2–17 MeV energy range, to the distribution measured experimentally by a silicon diode detector.**

***Index Terms*— Energy deposition, Geant4 (G4), Monte Carlo (MC) simulation, neutron irradiation, silicon diode, single-event effect (SEE).**

I. Introduction

MONTE Carlo (MC) tools are extensively used in the domain of radiation effects on electronics [1] and, more particularly, for high-energy accelerator applications. For the latter, MC codes for radiation effects are used mainly in two complementary ways: first, for simulating the complex radiation environment produced around the accelerator [2]–[4]; second, for simulating the interaction between such radiation environments and the microelectronic components. In the case of single-event effects (SEEs), this second type of simulation involves the scoring of the event-by-event energy deposition in micrometric volumes, representative of the SEE sensitive volumes (SVs). The key added value of such simulations with respect to the complementary experimental data is that they can provide the SEE probability as a result for a very broad range of particles and energies present in the accelerator environment and typically not accessible experimentally.

In the context of the Radiation to Electronics (R2E) project [5] at CERN, SEE MC simulations are extensively used in order to model e.g., the impact of high-Z materials on the energy dependence of the SEE response [6], the effect of nuclear interactions from heavy ions [7], the contribution of low-energy protons, and other singly charged particles to the overall SEU rate [8], as well as the $\pi^{\pm}$ SEE cross section and its impact on a mixed-field environment [9]. The primary MC tool used so far for such simulations was FLUKA [10], developed and distributed by CERN, and which is also the workhorse for calculations of the radiation environment around the accelerator.

Another important contribution to the mixed-field overall SEE rate, in addition to those introduced above, comes from so-called intermediate energy neutrons in the 0.2–20 MeV range [11]. As opposed to what occurs above 20 MeV, where, in first approximation, the hadronic SEE cross section can be considered constant as a function of energy [12], [13], neutron SEE responses in the intermediate energy range show a very strong energy dependence, which can vary significantly across different technologies. Therefore, there is a strong interest in applying MC tools to retrieve the behavior of SEE probabilities in this neutron energy range, further motivated by the difficulty of retrieving experimental results in this region. It is to be noted that such a neutron energy region is also highly relevant for other radiation environments, such as atmospheric, fission, fusion, and medical.

A number of MC simulation tools have been developed specifically for SEE simulations or applied for such simulations over the last decades [14]. For example, simulation frameworks, such as MRED [15], TIARA [16], and MUSCA SEP^3 [17], were developed for SEE simulations, but, unfortunately, none of these tools is open-source and accessible for public users. A version of MRED with limited capabilities is publicly accessible for use via the CRÈME-MC website [18], which does not support the simulation of neutrons. Other tools are complex, general-purpose MC codes, such as FLUKA, Geant4 (G4) [19], and MCNP(X) [20], all of which can be used for SEE simulations, but none of them has been developed or optimized for this specific purpose. Although FLUKA is used already successfully for SEE simulations at CERN with the help of an SEE scoring user routine [21], it can presently not be used to simulate neutron event-by-event energy deposition distributions below 20 MeV, as neutrons below this energy are treated by a multigroup algorithm, as opposed to via pointwise cross sections.

With the main motivation of overcoming such limitations, G4SEE, a toolkit based on G4 is being developed in the framework of the CERN R2E project. The toolkit is capable of simulating neutron-induced SEEs as well, and it has been

Manuscript received November 22, 2021; accepted January 27, 2022. Date of publication February 8, 2022; date of current version March 16, 2022. This work was supported by CERN.

Dávid Lucsányi, Rubén García Alía, Kacper Biłko, and Matteo Cecchetto are with CERN, 1211 Meyrin, Switzerland (e-mail: david.lucsanyi@cern.ch).

Salvatore Fiore is with the ENEA Frascati Research Center, 00044 Frascati, Italy.

Elisa Pirovano is with Physikalisch-Technische Bundesanstalt, 38116 Brunswick, Germany.

Color versions of one or more figures in this article are available at https://doi.org/10.1109/TNS.2022.3149989.

Digital Object Identifier 10.1109/TNS.2022.3149989

Fig. 1. Logo of the open-source G4SEE SEE simulation toolkit developed at CERN accessible via the https://cern.ch/g4see website.

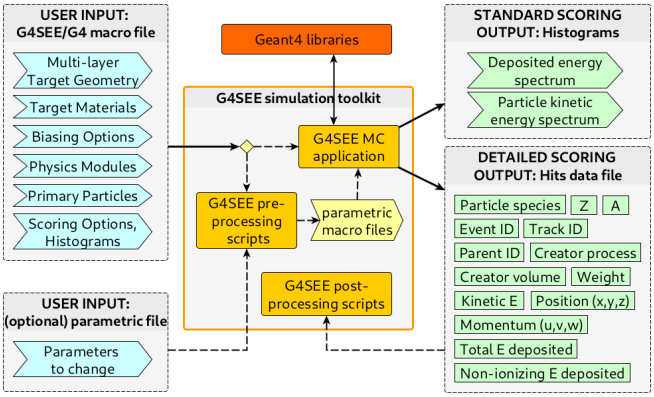

Fig. 2. High-level architecture of G4SEE toolkit listing the main user inputs and outputs. It includes two scoring options: standard and detailed scoring to extract all SEE related data event-by-event or particle-by-particle during the simulations.

released as a free and open-source code; thus, the radiation effects community can maintain it in the long term (see Fig. 1). The G4SEE toolkit is introduced in detail in Section II of this article. As mentioned above, the key observable retrieved from MC simulations for SEEs is the energy deposition distribution; therefore, in this work, it has been also obtained experimentally via a solid-state silicon detector setup introduced in Section III, along with the neutron test campaigns performed at ENEA FNG [22] and PTB PIAF [23] irradiation facilities with a broad range of monoenergetic neutrons (1.2–17 MeV). In Section IV, the experimental results are compared to those obtained via G4SEE, showing a satisfactory agreement. Detailed G4SEE simulations were performed and analyzed in Section V to better understand the contributions of various nuclear reactions to the overall energy deposition distributions. Finally, the conclusions and outlook of the work are included in Section VI.

II. G4SEE Toolkit for SEE Modeling

G4SEE enables an efficient, event-by-event, and particle-by-particle direct and indirect energy deposition scoring in micrometric volumes, allowing to extract all the information related to single events, which are relevant for and required by the user.

The development is driven by the needs of users and a diverse set of use cases; therefore, it is designed to be as flexible and general as possible within the simulations of SEEs. G4SEE is a free and fully open-source code, accessible via the https://cern.ch/g4see website, allowing the whole radiation effects community to be involved both as user and contributor of the toolkit. It is based on the latest two major G4 releases, currently versions 10.6 and 10.7.

The G4SEE toolkit includes the main G4 MC C++ application performing the particle transport simulations and several

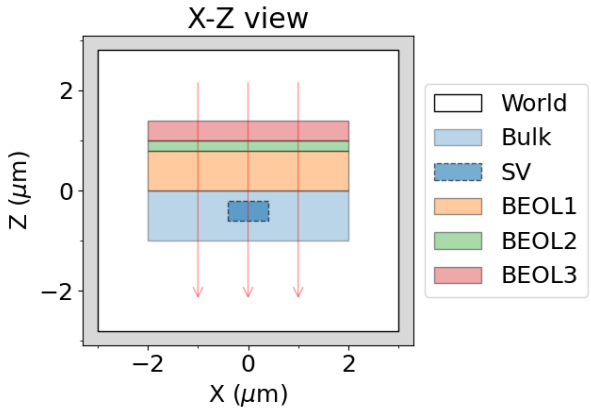

Fig. 3. Example of a user-defined multilayer target geometry of a microelectronic cell consisting of an SEE SV within bulk and three back end of line (BEOL) layers with user-defined materials.

supporting Python 3 scripts complementing the main MC application with preprocessing and postprocessing capabilities, all assembled together into a single toolkit. The high-level architecture of the toolkit with main user inputs and outputs is shown in Fig. 2. Inputs are at least one G4 style ASCII macro file with G4SEE specific macro commands (required) and a parametric configuration YAML file to change parameters run by run (optional). Outputs are user-defined deposited energy and particle kinetic energy histograms scored in user-defined geometry regions and written to ASCII files (optional). Moreover, with detailed scoring, all the requested quantities and information of individual particles scored per event can be written to a CSV output file line by line (optional). In the following part, the main features of G4SEE are briefly introduced.

For the target geometry, users can make use of NIST materials predefined by G4 [24] but also can define any custom material used in electronic components via macro commands: elements with user-defined isotope abundances, compounds consisting of various elements (e.g., Si_3N_4), or even mixtures of different materials.

The target geometry (either rectangular or cylindrical shaped) consists of a bulk volume and the arbitrary number of optional BEOL layers, as one can see in Fig. 3. Inside the Bulk volume, an SV is defined. All dimensions, relative positions, and materials of these volumes are user-defined. Currently, only a single SV can be defined with either a rectangular parallelepiped (RPP) or cylinder shape, which could limit use cases, but this will change in future releases, as a more general geometry definition will be implemented enabling the use of complex-shaped SVs in arbitrary number, even nesting them together [25]. No limitations related to the use of the RPP model for the SV or its dimensions are known yet based on previous MC simulation works that already successfully applied the RPP model for deep submicrometer (65 and 40 nm SRAMs) technologies in the case of protons [13] and neutrons [26].

G4 has a large set of physics models structured in optional predefined modules and physics lists on the highest level. Building on this modularity and freedom of choice, G4SEE

allows the users to build their own physics from various electromagnetic (EM), hadron elastic, hadron inelastic, and ion physics modules [27], [28], simply selecting the best set of options for their specific simulation case. For SEE simulations, it is recommended to use the most accurate EM physics module *EM_option4*. The *MicroElec* models [29] can also be chosen, up to now only for silicon, but soon for another ten materials as well [30]. For neutrons below 20 MeV, the modules containing high-precision (HP) neutron models are the recommended options. Moreover, the particle production range (or energy) cuts for $e^{\pm}$, γ, and all hadrons can be also set, which is very useful in reducing the computational time, if applicable.

In order to study the energy deposition by inelastic interactions with low probabilities, a generic, physics-based microscopic cross section biasing [24] is implemented in G4SEE to artificially multiply the occurrence of specific interactions by an arbitrary factor, which is then corrected for in the scoring. Different interaction types of all particle species can be biased, currently excluding only $Z > 2$ heavy ions. By default, biasing is applied for primary particles, but this can be extended to secondaries too, and it can be selectively enabled or disabled in any volume of the target geometry.

The *General Particle Source (GPS)* G4 class [24] is used by the application, enabling the users to simply define an arbitrary primary particle source with any energy spectrum, angular distribution, and beam shape.

G4SEE allows users to extract and save to an ASCII file all physics data distributions used internally by G4 to simulate particle transport without the need of running a simulation. This feature, like all the others, can be enabled via macro commands. It could be relevant for SEE studies and tests, such as dE/dx (LET or stopping power), range of particles, and microscopic and macroscopic cross sections of particle interactions.

The most important features of G4SEE regarding SEE simulations are the scoring mechanisms, namely, the standard and detailed scoring. Using standard scoring, currently, two quantities can be scored: the first and most important is the total energy deposited per event (E_{dep}) inside the whole SV (event-by-event scoring), and the second is the kinetic energy (E_{kin}) of selected particle species when entering or produced inside the SV (particle-by-particle scoring). These quantities are saved in user-defined histograms with linear or logarithmic binning and printed to ASCII histogram files. Then, the E_{dep} histogram files can be used, for example, to calculate the reverse cumulative sum of energy deposited in order to retrieve the SEE cross section as a function of the critical charge.

With the detailed scoring, users can score all particle hits in the SV, i.e., information of individual particles when entering or produced in SV (particle-by-particle scoring). All the following data of each particle can be printed in a single line of a CSV output file: particle species, event ID, particle (track) ID, parent particle ID, atomic and nucleon numbers, position and momentum coordinates, kinetic energy, inverse biasing weight, creator process, creator volume, total energy deposited, and total non-ionizing energy deposited by that specific particle inside SV. By default, all e^-, e^+, and γ particles are grouped together per event, summing their energy deposition in order to reduce the verbosity and size of the output file. Optionally, one can set a kinetic energy threshold, so the particle grouping only happens for particles below this threshold, while the e^-, e^+, and γ particles with higher kinetic energy are scored and printed individually to the output file. In this way, individual scoring of all γ, e^-, and e^+ is also possible. Another, special $e^{\mp}$ grouping feature is also implemented, allowing them to group them by the particle ID of their closest nonelectron ancestor within events. For example, when a primary neutron produces a secondary α and ^{26}Mg nucleus within SV, the energy deposited directly by ionized electrons is added to the contributions of α and ^{26}Mg separately. Using this feature, it is possible to categorize single events by the main secondary products (proton, α, heavier fragments, and so on) produced or the nuclear reactions that occurred and analyze how much total energy was deposited by each particle directly and indirectly including also the contribution of all of its descendant particles (mostly secondary and tertiary ionization electrons).

There are additional preprocessing and postprocessing Python 3 scripts within the toolkit supporting G4SEE users with auxiliary capabilities. G4SEE is a multithreaded G4 application, capable of running on any number of CPU threads at the same time. Via its preprocessing script, it can be also run in the multiprocessing mode by submitting any number of parallel jobs to independent computing cluster nodes. Then, these cluster queue jobs can be monitored or deleted as well using the script. A parametric G4SEE run with varying a set of input parameters (e.g., particle energy and SV dimensions) can be also started, allowing to perform SEE parametric or sensitivity studies defining any setting in the macro file as a variable. In both multithreading and multiprocessing modes, a number of independent output histogram files are generated simultaneously, which then are merged into a single histogram file by the postprocessing script. Furthermore, there are scripts for visualizing the geometry defined in the macro file, plotting output histogram files, and processing a large amount of particle data saved to CSV output files using detailed scoring. With the latter, one can count the number of various secondary particles, their creator processes, and volumes where they were produced, as well as sum up the E_{dep} distribution of events based on the different groups of produced secondary particles or nuclear reactions (see a specific use case in Section V).

Cross-platform G4SEE Docker images are also available, which makes it possible for users to easily and quickly start a Docker container locally with the latest G4 and G4SEE already installed inside ready to use; thus, neither G4 installation nor G4SEE compilation is necessary to use it.

III. Experimental Measurements With a Silicon Diode Detector

Measurements and simulations of neutron energy deposition spectra in silicon diode detectors have been published already, irradiating the diode with various monoenergetic fast neutron beams between 24 and 100 MeV [31], [32]. The experimental work presented here complements these previous works at lower neutron energies using a silicon diode setup with a

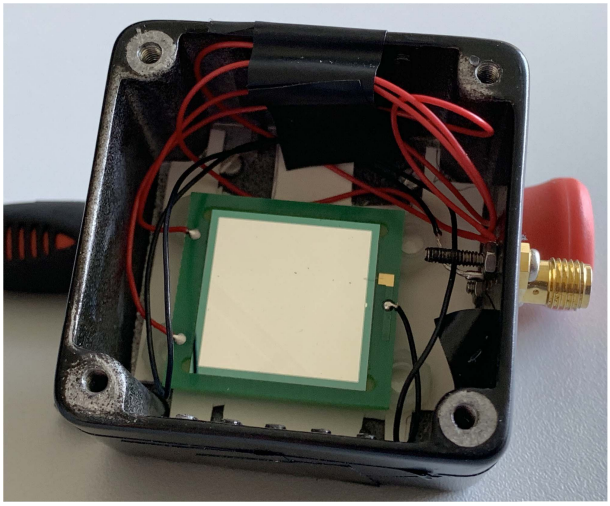

Fig. 4. Used 300 μm-thick n-type silicon diode (Micron MSX04 model) with 20 mm $\times$ 20 mm active area, mounted inside an aluminum case with 2.7 mm wall thickness, and operated fully depleted at -120 V bias voltage.

significantly higher energy resolution, while it gives results in good agreement with them.

A. Experimental Setup

The experimental setup used to benchmark the G4SEE event-by-event energy deposition distributions is shown in Fig. 4 and consisted of a silicon n-type diode (model MSX04) manufactured by Micron Semiconductor Ltd., encapsulated in an aluminum housing with 2.7 mm wall thickness. The silicon dimensions are 20 mm $\times$ 20 mm $\times$ 0.3 mm with a metallization layer of 500 nm of sputtered aluminum. The diode was operated fully depleted in the reversed bias mode at -120 V with its signal amplified through the CIVIDEC C2 low-noise current amplifier (2 GHz analog bandwidth and $g = 43.9$ dB measured gain). The signal was acquired through the CAEN DT5751 digitizer. The deposited energy E_{dep} of each event was calculated as the integral of the measured diode current $I(t)$ over time [see (1)] with the assumption that, on average, $E_{e-h} = 3.6$ eV energy is needed to create one electron–hole pair via ionization

$$E_{\text{dep}} = \frac{E_{e-h}}{g} \int I(t)dt. \tag{1}$$

B. Neutron Irradiation Test Campaign at FNG

Using the setup described above, a neutron irradiation test was performed at the Frascati Neutron Generator (FNG) Facility [22] of the ENEA Institute in Italy (see Fig. 5). Via the ^{3}H(d, n)^{4}He nuclear reaction, a 14.8 MeV monoenergetic spectrum of neutrons was obtained (at 0°) with a $\sigma_E \approx 276$ keV standard deviation and with an average flux of $9 \cdot 10^6$ cm^{-2}s^{-1} at the diode (at 7.6 cm from the target), resulting in a total fluence of $2.7 \cdot 10^9$ cm^{-2} over a $\sim$300 s long irradiation (see Table I).

The measured energy deposition spectrum is plotted in Fig. 7. Below certain energy, data were not acquired by setting an acquisition threshold with the digitizer in order to limit the number of events preventing saturation of the digitizer buffer. The acquisition threshold was changed run by run.

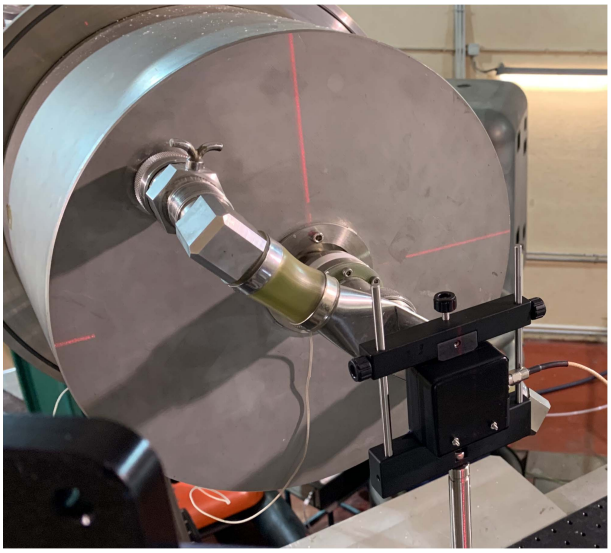

Fig. 5. Experimental test setup at the ENEA FNG Facility [22] irradiated with 14.8 MeV monoenergetic neutron flux produced in ^{3}H(d, n)^{4}He nuclear reaction.

TABLE I

NUCLEAR REACTION USED, NEUTRON ENERGY (E_n), STANDARD DEVIATION OF NEUTRON ENERGY (σ_E), DIODE DISTANCE FROM SOURCE (d), AVERAGE FLUX ($\langle\varphi\rangle$), AND TOTAL FLUENCE (Φ) VALUES AT THE POSITION OF THE Si DIODE FOR THE VARIOUS TEST RUNS AT FNG AND PIAF (PTB)

Facility, Reaction	E_n (MeV)	σ_E (keV)	d (cm)	$\langle\varphi\rangle$ (cm^{-2}/s)	Φ (cm^{-2})
PIAF, ^{3}H(d,n)	17	154	11.3	$1.18{\cdot}10^5$	$1.11{\cdot}10^8$
FNG, ^{3}H(d,n)	14.8	276	7.6	$9.01{\cdot}10^6$	$2.74{\cdot}10^9$
PIAF, ^{2}H(d,n)	8	85	12.4	$7.41{\cdot}10^5$	$3.61{\cdot}10^8$
PIAF, ^{2}H(d,n)	5	85	12.4	$1.73{\cdot}10^5$	$2.65{\cdot}10^8$
PIAF, ^{3}H(p,n)	2.5	54	11.3	$4.12{\cdot}10^5$	$4.51{\cdot}10^8$
PIAF, ^{3}H(p,n)	1.2	39	11.3	$3.44{\cdot}10^5$	$2.48{\cdot}10^8$

C. Neutron Irradiation Test Campaign at PIAF

Similar tests described above have been also performed at the Physikalisch-Technische Bundesanstalt (PTB) Ion Accelerator Facility (PIAF) [23] in Germany (see Fig. 6). To produce different neutron beams, the following nuclear reactions (and targets) were used: ^{3}H(d, n)^{4}He reaction for 17 MeV (Ti(^{3}H) target), a ^{2}H(d, n)^{3}He reaction for 8 and 5 MeV ($^2H_2$ gas target), and ^{3}H(p, n)^{3}He reaction for 2.5 and 1.2 MeV energies (Ti(^{3}H) target). Note that the neutron fields are monoenergetic, as detailed in [26]. The standard deviations of neutron energies are reported in [23]. The diode was placed either at 11.3 or 12.4 cm of distance from the target, and the fluence ranged from $1.1 \cdot 10^8$ to $4.5 \cdot 10^8$ cm^{-2} depending on the run, as listed in Table I. A significant difference in the setup with respect to that used in FNG was the use of a $\sim$250 μm PVC tape attached inside the Al lid box containing the diode, which had a nonnegligible effect on the acquired data. The run with 17 MeV neutrons had an additional Al plate of 0.5 mm in between the diode and the neutron source, as shielding against the protons generated by the parasitic ^{3}He(d, p)^{3}H reaction

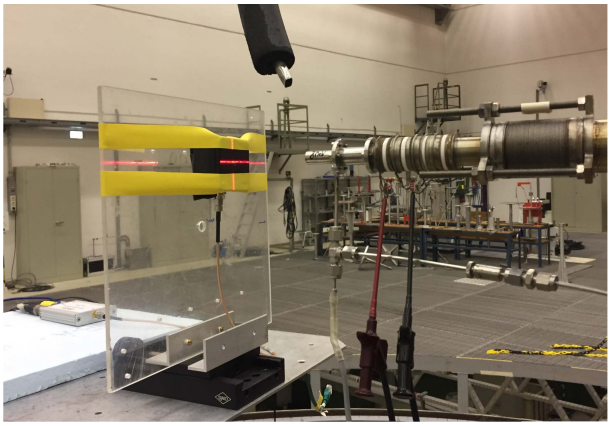

Fig. 6. Experimental test setup at the PIAF [23], irradiated with 17, 8, 5, 2.5, and 1.2 MeV monoenergetic neutron fluxes using Ti(^{3}H) and $^2H_2$ targets as neutron source.

with the ^{3}He nuclei resulting from the β decay of ^{3}H in the target.

The measured energy deposition spectra are plotted in Fig. 7. The data acquisition threshold of each PIAF run was lower than that during the FNG test due to the lower neutron fluxes. Although a test run with 144 keV neutrons was also performed, it was not used since the acquired data contained only γ background above the threshold based on the simulation results and feedback from the facility operators (mainly 478 keV γ decay photons of the ^{7}Li first excited state). The 1.2 MeV neutron field also had some γ contribution from excited ^{109}Ag nuclei (311 and 415 keV) and a γ continuum up to ~1.2 MeV, which can be also seen on the 1.2 MeV E_{dep} spectrum of Fig. 7.

IV. Validation of G4SEE With Experimental Data

As mentioned in Section I, the key observable for SEE simulations is the energy deposition distribution, which has been measured experimentally with the setup described in Section III. Hereinafter, test results are compared to G4SEE simulation results to demonstrate the capabilities and validate the accuracy of the tool. Experimental validation of G4SEE in order to reassure users of its accuracy and error-free operation is essential. Furthermore, in the case of SEE energy deposition studies, due to the usually unknown, complex structures, and large uncertainties of the simulated microelectronic components (micrometric geometries, materials, doping profile, critical charge, and so on), proven reliability in the simulation tool is even more required by the users.

Although in terms of SEE simulations, a very large (few hundred μm) SV is not representative of complex, deep submicrometer electronic structures (especially from dimensions and charge collection aspects), a validation approach using a Si diode with large SV has been applied in this work as the first attempt to validate G4SEE, and indirectly G4 physics models. The main reason for this choice is to reduce the abovementioned uncertainties by irradiating a fully depleted Si PN diode with a known, simple planar geometry, and a pure, homogeneous silicon material without any packaging or unknown BEOL layers. Furthermore, measuring event-by-event energy deposition distributions directly in small structures (e.g., SRAM transistors) is much more difficult or even unfeasible.

Later, validation for deep submicrometer technologies will be performed as well since it is already proven that FLUKA and G4 MC simulation tools can be successfully used for SEE simulations at least down to 40 nm SRAM technologies [13], [26], and G4 is continuously evolving further in this field [29], [30].

A. G4SEE Simulations of the Experimental Setups

The FNG and PIAF experimental test setups and all the test runs have been simulated using G4SEE, reproducing them in G4SEE macro files to reflect the experimental conditions as accurately as known and reasonably achievable.

The 20 mm × 20 mm detector SV was defined as a 299 μm layer in the center of a 300 μm Si bulk with a 500 nm Al metallization on top. A 2 cm air gap and a 2.7 mm Al housing lid with a 250 μm PVC tape on the inside or outside surface were added depending on the test run. The effects of the 2 mm-diameter hole covered by the PVC tape in the center of the Al housing lid were negligible in the preliminary simulation results and are, therefore, ignored hereinafter.

Inside the SV, cross section biasing has been applied for primary neutrons with a factor of 1000 for all types of neutron interactions (elastic, inelastic, and capture), while, in other layers of the geometry, no biasing was applied. Results of biased (nonanalog) and nonbiased (analog) runs have been compared to make sure that the same distributions are obtained but with better statistics and lower standard deviation per bin in the biased case, showing that the precision can be increased without compromising the accuracy.

Additional to the default *EM_option4* physics, the *ElasticPhysicsHP* hadron elastic and *FTFP_BERT_HP* hadron inelastic physics modules were applied, both including the HP neutron models, which are primarily used in this specific case. HP neutron models of G4 [28] simulate the interactions of neutrons with kinetic energy below 20 MeV, down to thermal energies. These include radiative capture, elastic scattering, fission, and inelastic scattering processes. HP models use neutron cross section data derived from the ENDF/B-VI evaluated data library, which is treated as pointwise cross sections, explicitly including all neutron nuclear resonances. HP models result in a set of secondary particles produced by a low-energy neutron, which are further tracked by G4, and deposit energy in the SV. The following production range cuts were set for secondary particles: 1 mm for γ, 1 μm for $e^{\mp}$, and 100 nm for all other particles.

In the case of the FNG run, an isotropic point source of primary neutrons has been defined at 7.6 cm from the surface of the Si diode (5.3 cm from the surface of the Al lid), resulting in a 21.25° total view angle in the diagonal of the diode. Primary neutrons had a Gaussian spectrum with 14.8 MeV mean energy and $\sigma_E = 276$ keV standard deviation. The same steps were followed in the case of the PIAF runs, using run-specific distances, neutron energy mean, and standard

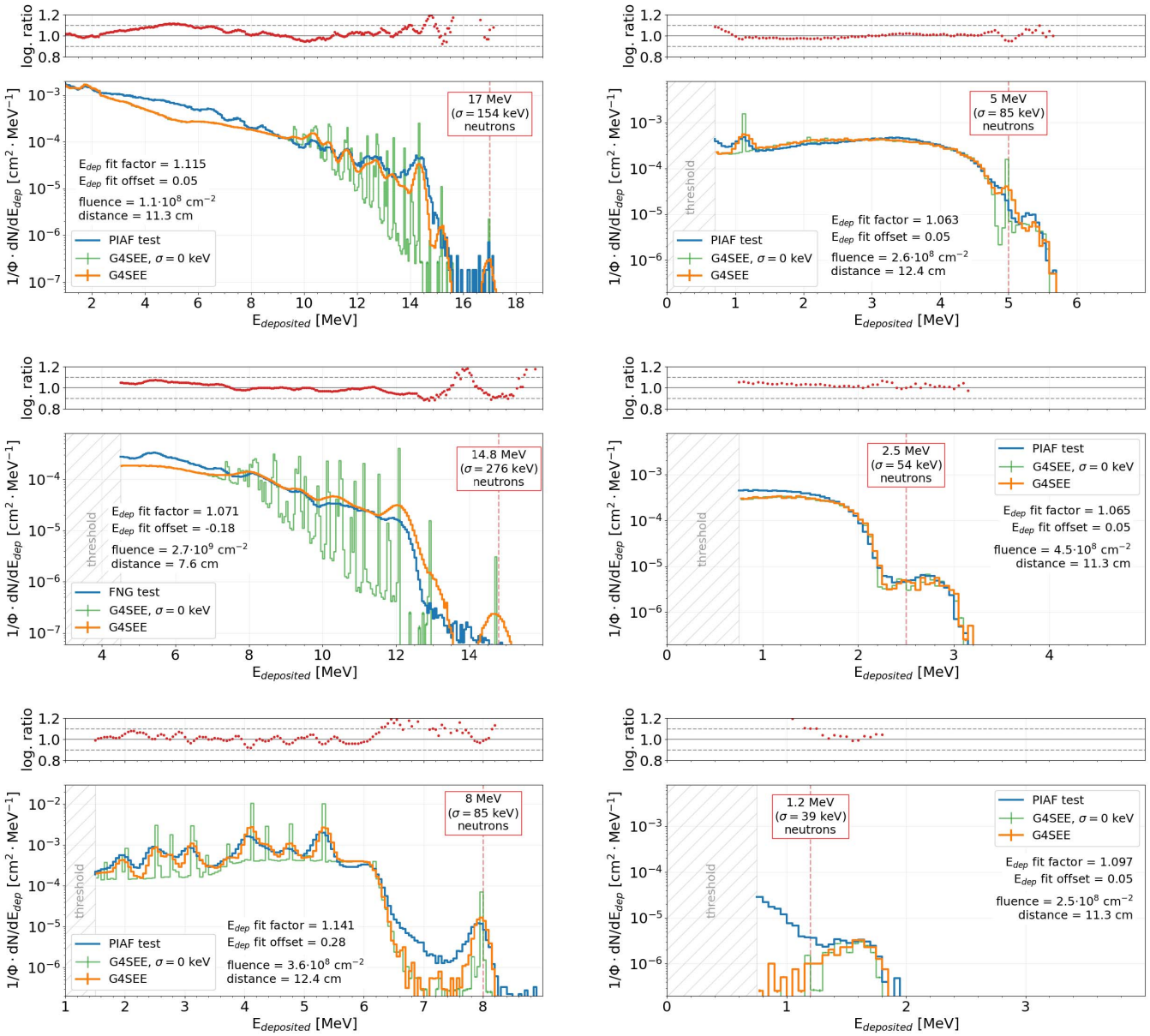

Fig. 7. Comparison of energy deposition distributions (fluence-normalized differential counts in function of deposited energy) measured with the diode at PIAF and FNG facilities (blue) and simulated using G4SEE (orange) with 17, 14.8, 8, 5, 2.5, and 1.2 MeV neutrons. Simulated spectra with $\sigma_E = 0$ keV are also added (green). Logarithmic count ratios of measured and simulated distributions are plotted as well, showing the good agreement between them over several orders of magnitude.

deviation values. Simulations with $\sigma_E = 0$ keV neutron energy standard deviation were also performed.

B. Comparison of Simulated and Experimental Data

G4SEE simulations with standard scoring were run in order to obtain the total deposited energy per event (E_{dep}) spectra for the detector SV. The total E_{dep} includes contributions of all particles (including secondary and tertiary) summed up and added to the histogram event by event. The total E_{dep} is the sum of both ionizing and nonionizing energy deposited as defined by G4. The nonionizing energy deposited is usually the smaller fraction of the total energy deposited by recoil Si nuclei after ^{x}Si(n, n)^{x}Si elastic or ^{x}Si(n, n$'$)^{x}Si inelastic interactions, which does not contribute to the experimental or simulated total E_{dep} spectra above the acquisition threshold at all. The only exception is the 17 MeV run, where recoil Si nuclei contribute to E_{dep} spectrum above acquisition threshold due to the relatively low threshold and can deposit part of their energy loss as nonionizing energy, but this is only ∼10% of their total energy loss below ∼2.3 MeV maximum Si kinetic energy [33] and, therefore, negligible.

The E_{dep} total deposited energy spectra are directly compared to the acquired experimental test data after normalization, as plotted in Fig. 7. Histograms are normalized by the fluence and the energy bin width, resulting in

fluence-normalized differential count distributions in the function of E_{dep}. Measured E_{dep} distributions have been fit horizontally (along the deposited energy axis) to overlap simulated distributions on a logarithmic scale with the help of an E_{dep} fit scaling factor and offset since both the experimental and simulated data have several uncertainties, all contributing to the systematic error of the difference between measured and simulated E_{dep}. The largest experimental uncertainties and variations are the average neutron fluxes provided by the facilities, the standard deviation of neutron energy, the mean electron–hole pair creation energy in the diode, amplifier gain, and measured source-diode distance values. The simulation uncertainties are secondary background particle fluxes, materials missing from the simulation, and the diode SV geometry, and may include missing or inaccurate microscopic cross section data of G4 HP neutron models for certain nuclear reactions. All of these together cause a slight scaling and offset of the measured E_{dep} data relative to simulated data depending on the test run. Fit scaling factors and offsets used are shown on each plot in Fig. 7. Although the 8 MeV test run has the highest E_{dep} scaling factor (1.14, i.e., 14% increase in E_{dep}) and offset (280 keV) in the experimental data to fit the simulated results, after applying the correction, the measured histogram fits well with the simulated histogram, resulting in one of the best overlaps, so G4SEE well reproduces the shape and most E_{dep} peaks of the experimental distributions. The two test runs with the lowest factors and offsets are the 5 MeV (6.3%, 50 keV) and 2.5 MeV (6.5%, 50 keV) neutron runs.

After fitting the histograms to correct for the small systematic errors, a logarithmic count ratio was plotted as well in Fig. 7, which is calculated as $\log_{10}$(Sim. data)/$\log_{10}$(Exp. data) in the function of E_{dep}, showing discrepancy on the logarithmic scale. In most cases, the logarithmic count ratio is close to 1 and within the [0.9, 1.1] interval over wide energy ranges, meaning that the logarithm values of experimental and simulated counts differ in less than 10%, which is acceptable when comparing MC simulation and experimental data over four to five orders of magnitude. In some cases, experimental data have much fewer statistics than simulations, especially at low probability and high E_{dep} peaks (like 17 and 14.8 MeV), causing higher than 1.1 logarithmic count ratios. Other discrepancies in differential counts at given E_{dep} values are due to peaks or backgrounds missing from the simulation caused by known and unknown secondary incident particle fluxes, including, but not limited to, γ background (e.g., 1.2 MeV run) and parasitic nuclear reactions in the target (e.g., 17 MeV run). Secondary particles from known upstream DUT material layers (described in Section III) are included in the simulation, such as protons from the PVC tape (e.g., 8 MeV run).

By integrating the differential count distributions above the acquisition thresholds, the total number of collected events was calculated (normalized by the fluence) and compared for each run (see Table II). Ratios of the measured and simulated events are close to 1 in both 5 and 8 MeV runs (<2% difference), the difference is 27%–32% for 2.5 , 14.8, and 17 MeV runs, and 526% for 1.2 MeV due to the γ background.

TABLE II
COMPARISON OF TOTAL NUMBER OF EVENTS MEASURED BY THE Si DIODE AND SCORED BY G4SEE ABOVE THRESHOLD (ENERGY INTEGRAL OF THE FLUENCE-NORMALIZED DIFFERENTIAL COUNT DISTRIBUTIONS)

E_n (MeV)	Threshold (MeV)	Measured (cm^2)	Simulated (cm^2)	Measured / Simulated
17	1.0	$6.26 \cdot 10^{-3}$	$4.78 \cdot 10^{-3}$	1.311
14.8	4.5	$9.82 \cdot 10^{-4}$	$7.73 \cdot 10^{-4}$	1.271
8	1.5	$3.17 \cdot 10^{-3}$	$3.23 \cdot 10^{-3}$	0.984
5	0.7	$1.37 \cdot 10^{-3}$	$1.38 \cdot 10^{-3}$	0.999
2.5	0.75	$4.91 \cdot 10^{-4}$	$3.70 \cdot 10^{-4}$	1.327
1.2	0.75	$9.10 \cdot 10^{-6}$	$1.45 \cdot 10^{-6}$	6.266

As discussed above, after correcting for small systematic E_{dep} distribution errors and disregarding high background and peaks with low experimental statistics, the overall agreement between measurements and simulations is satisfactory (see Fig. 7) both in terms of the fluence-normalized differential counts (along the y-axis) and energy deposition per event values (along the x-axis). G4SEE reproduces well the acquired test data within errors, hence providing confidence in G4SEE when applying it to neutron SEE energy deposition studies in micrometric geometries.

Simulated E_{dep} spectra of monoenergetic neutrons with $\sigma_E = 0$ keV standard deviation were also added to the figures to show the energy levels and intensities of the distinct nuclear reaction channels in silicon and better understand the structure of the spectra. The various peaks in E_{dep} spectra correspond to a single or even multiple different excitation states of nuclei after (n, α) or (n, p) inelastic interactions. After an inelastic reaction, the higher energy level excitation state a nucleus has (e.g., ^{25}Mg has 12 different energy level excited states), the less energy can be deposited through ionization by the other secondary product (α in the case of ^{25}Mg) in that particular event [34]. Although the excited nucleus rapidly decays, the γ energy typically leaves the diode. Because of these, one can resolve several individual peaks in the E_{dep} spectrum related to the same nuclear reaction, as one can see also in Fig. 8.

V. SIMULATIONS WITH G4SEE DETAILED SCORING

In addition, G4SEE simulations with detailed scoring were also run and analyzed in order to acquire a detailed list of individual secondary particles and their scored values, such as the total energy deposited by them. The total deposited energy of the events has been grouped by the set of secondary particles produced event by event. The materials in the simulation had natural isotope abundances. The interacting isotopes and nuclear interactions cannot be scored directly, but these have been concluded based on the reaction products and baryon conservation. In Fig. 8, E_{dep} distributions of the four major nuclear interactions with the largest contributions are plotted. In the case of 14.8 MeV FNG run, most of the nuclear interactions induced by neutrons are ^{x}Si(n, n)^{x}Si elastic in 47.6% and ^{x}Si(n, n′)^{x}Si inelastic in 25.8%, which events are shown in the figure together combined. The remaining major inelastic interactions, depositing higher energies, are the following: ^{28}Si(n, p)^{28}Al (13.7%), ^{28}Si(n, α)^{25}Mg (10.8%),

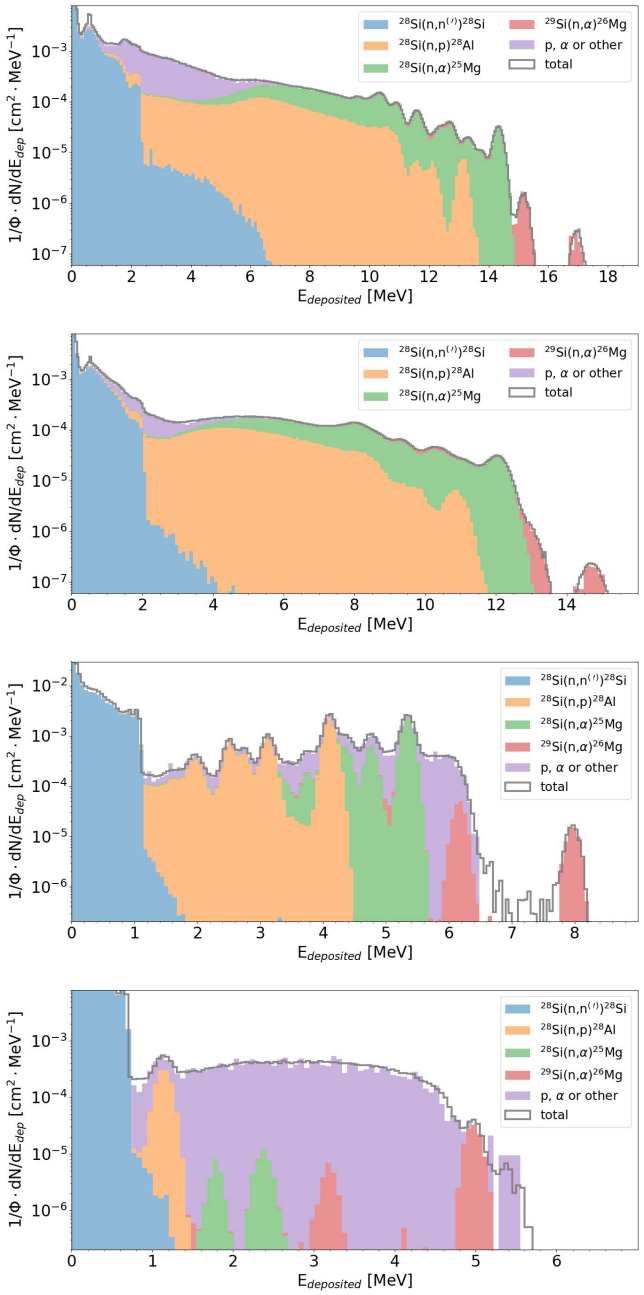

Fig. 8. Neutron energy deposition spectra at 17, 14.8, 8, and 5 MeV energies were simulated using G4SEE detailed scoring feature and analyzed with G4SEE postprocessing script. The E_{dep} values per particle have been summed up by the secondary particle product groups per event, clearly showing which inelastic or elastic nuclear reaction occurred event by event. The main contributors to total E_{dep} distribution (gray) are the nuclear reactions producing ^{28}Si (blue), ^{28}Al (orange), ^{25}Mg (green), and ^{26}Mg (red). Events when no nucleus (heavier than α) scored during simulation (purple) contribute significantly at lower neutron energies.

^{29}Si(n, α)^{26}Mg (0.4%), and ^{29}Si(n, p)^{29}Al (0.4%). The highest energy is deposited in the Si diode by the products of the ^{29}Si(n, α)^{26}Mg reaction, and ^{25}Mg and ^{28}Al isotopes have the most excitation states and, therefore, peaks in the final E_{dep} distributions.

It is important to highlight the events in which no heavy nucleus ($A > 4$) is scored within SV, only other secondaries ($A \leq 4$), mainly proton, α, and neutron particles from inelastic reactions (their contribution is shown in purple in Fig. 8). The reason is that either no heavy nucleus is produced (e.g., due to production range cut) or the nucleus could not reach SV to be printed in the detailed scoring Hits file (e.g., due to stopping in Al metallization or dead layer of Si diode). During PIAF test runs and simulations, especially at lower energies, a significant number of protons entered the Si diode from the PVC tape located on the inner surface of the Al lid. Both the effect and contribution of protons can be investigated and understood with G4SEE, especially with its detailed scoring feature. Although neutron environments of the Si diode at PIAF were not pure neutron fields because of the tape, G4SEE and G4 well reproduced the measured distributions and confirmed the accuracy for neutron SEE studies and applications.

VI. Conclusion and Outlook

G4SEE, an MC SEE simulation toolkit, has been developed for the radiation effect community to benefit from the particle transport capabilities of G4 in SEE simulation studies, especially in the case of low and intermediate energy neutrons below 20 MeV. G4SEE is a free and open-source code, accessible via the https://cern.ch/g4see website.

The energy deposition distributions by 17, 14.8, 8, 5, 2.5, and 1.2 MeV neutrons from the PIAF and ENEA FNG have been successfully measured with a 300 μm-thick silicon diode detector. Then, the experiments were simulated using G4SEE, resulting in energy deposition distributions in good agreement with the experimentally measured data, demonstrating capabilities, and validating the accuracy of G4SEE for neutron-induced SEE simulations in large SVs and a broad neutron energy range between 1.2 and 17 MeV.

Beyond large SVs and monoenergetic neutrons, further validation activities are ongoing and will be published as well, regarding simulations and SEE rate calculations for various small SVs, including deep submicrometer technologies, as well as comparisons with both neutron, proton, heavy ion, and γ irradiation test results.

In parallel, G4SEE development is continuously ongoing based on the needs of the user community. The next major features to be implemented are nested SVs with different weight factors, pixelated and periodic geometries, user-defined electric fields, and modeling electrical signal readout.

Acknowledgment

The authors would like to thank the access to the PIAF and FNG irradiation facilities, and all the technical and scientific support provided by Ralf Nolte at PTB.

References

[1] R. A. Weller *et al.*, "General framework for single event effects rate prediction in microelectronics," *IEEE Trans. Nucl. Sci.*, vol. 56, no. 6, pp. 3098–3108, Dec. 2009.

[2] R. G. Alía *et al.*, "LHC and HL-LHC: Present and future radiation environment in the high-luminosity collision points and RHA implications," *IEEE Trans. Nucl. Sci.*, vol. 65, no. 1, pp. 448–456, Jan. 2018.

[3] A. Lechner *et al.*, "Validation of energy deposition simulations for proton and heavy ion losses in the CERN large hadron collider," *Phys. Rev. A, Gen. Phys.*, vol. 22, Jul. 2019, Art. no. 071003.

[4] K. Bilko *et al.*, "Radiation environment in the LHC arc sections during run 2 and future HL-LHC operations," *IEEE Trans. Nucl. Sci.*, vol. 67, no. 7, pp. 1682–1690, Jul. 2020.

[5] *CERN Radiation To Electronics (R2E)*. Accessed: 2021. [Online]. Available: https://r2e.web.cern.ch

[6] R. G. Alía *et al.*, "Energy dependence of tungsten-dominated SEL cross sections," *IEEE Trans. Nucl. Sci.*, vol. 61, no. 5, pp. 2718–2726, May 2014.

[7] V. Wyrwoll *et al.*, "Heavy ion nuclear reaction impact on SEE testing: From standard to ultra-high energies," *IEEE Trans. Nucl. Sci.*, vol. 67, no. 7, pp. 1590–1598, Jul. 2020.

[8] R. G. Alia *et al.*, "Direct ionization impact on accelerator mixed-field soft-error rate," *IEEE Trans. Nucl. Sci.*, vol. 67, no. 1, pp. 345–352, Jan. 2020.

[9] A. Coronetti *et al.*, "The pion single-event effect resonance and its impact in an accelerator environment," *IEEE Trans. Nucl. Sci.*, vol. 67, no. 7, pp. 1606–1613, Jul. 2020.

[10] G. Battistoni *et al.*, "Overview of the FLUKA code," *Ann. Nucl. Energy*, vol. 82, pp. 10–18, Aug. 2015.

[11] M. Cecchetto, R. G. Alía, S. Gerardin, M. Brugger, A. Infantino, and S. Danzeca, "Impact of thermal and intermediate energy neutrons on SRAM SEE rates in the LHC accelerator," *IEEE Trans. Nucl. Sci.*, vol. 65, no. 8, pp. 1800–1806, Aug. 2018.

[12] K. Roeed *et al.*, "Method for measuring mixed field radiation levels relevant for SEEs at the LHC," *IEEE Trans. Nucl. Sci.*, vol. 59, no. 4, pp. 1040–1047, Aug. 2012.

[13] A. Coronetti *et al.*, "Assessment of proton direct ionization for the radiation hardness assurance of deep submicron SRAMs used in space applications," *IEEE Trans. Nucl. Sci.*, vol. 68, no. 5, pp. 937–948, May 2021.

[14] R. A. Reed *et al.*, "Anthology of the development of radiation transport tools as applied to single event effects," *IEEE Trans. Nucl. Sci.*, vol. 60, no. 3, pp. 1876–1911, Jun. 2013.

[15] R. A. Reed *et al.*, "Physical processes and applications of the Monte Carlo radiative energy deposition (MRED) code," *IEEE Trans. Nucl. Sci.*, vol. 62, no. 4, pp. 1441–1461, Aug. 2015.

[16] P. Roche, G. Gasiot, J. L. Autran, D. Munteanu, R. A. Reed, and R. A. Weller, "Application of the TIARA radiation transport tool to single event effects simulation," *IEEE Trans. Nucl. Sci.*, vol. 61, no. 3, pp. 1498–1500, Jun. 2014.

[17] G. Hubert, S. Duzellier, C. Inguimbert, C. Boatella-Polo, F. Bezerra, and R. Ecoffet, "Operational SER calculations on the SAC-C orbit using the multi-scales single event phenomena predictive platform (MUSCA SEP3)," *IEEE Trans. Nucl. Sci.*, vol. 56, no. 6, pp. 3032–3042, Dec. 2009.

[18] J. H. Adams. (2021). *Crème*. [Online]. Available: https://creme.isde.vanderbilt.edu

[19] J. Allison *et al.*, "Recent developments in Geant4," *Nucl. Instrum. Methods Phys. Res. A, Accel. Spectrom. Detect. Assoc. Equip.*, vol. 835, pp. 186–225, Nov. 2016.

[20] T. Goorley *et al.*, "Initial MCNP6 release overview," *Nucl. Technol.*, vol. 180, no. 3, pp. 298–315, 2012.

[21] R. G. Alía, "Radiation fields in high energy accelerators and their impact on single event effects," Ph.D. dissertation, Inst. Electron. South, Inf., Struct. Syst., Univ. Montpellier 2, Montpellier, France, Dec. 2014. [Online]. Available: https://cds.cern.ch/record/2012360

[22] A. Pietropaolo *et al.*, "The Frascati neutron generator: A multipurpose facility for physics and engineering," *J. Phys., Conf. Ser.*, vol. 1021, May 2018, Art. no. 012004.

[23] S. Röttger *et al.*, "The PTB neutron reference fields (PIAF)–quasi–monoenergetic neutron reference fields in the energy range from thermal to 200 MeV," *AIP Conf. Proc.*, vol. 1175, no. 1, pp. 375–381, 2009.

[24] Geant4 Collaboration. *Geant4, Book For Application Developers, Release 10.7*. Accessed: Dec. 4, 2020. [Online]. Available: https://geant4.web.cern.ch/support/user_documentation

[25] K. M. Warren *et al.*, "Application of RADSAFE to model the single event upset response of a 0.25 μm CMOS SRAM," *IEEE Trans. Nucl. Sci.*, vol. 54, no. 4, pp. 898–903, Oct. 2007.

[26] M. Cecchetto *et al.*, "0.1–10 MeV neutron soft error rate in accelerator and atmospheric environments," *IEEE Trans. Nucl. Sci.*, vol. 68, no. 5, pp. 873–883, May 2021.

[27] Geant4 Collaboration. *Geant4, Guide For Phys. Lists, Release 10.7*. Accessed: Dec. 4, 2020. [Online]. Available: https://geant4.web.cern.ch/support/user_documentation

[28] Geant4 Collaboration. *Geant4, Phys. Reference Manual, Release 10.7*. Accessed: Dec. 4, 2020. [Online]. Available: https://geant4.web.cern.ch/support/user_documentation

[29] A. Valentin, M. Raine, M. Gaillardin, and P. Paillet, "Geant4 physics processes for microdosimetry simulation: Very low energy electromagnetic models for protons and heavy ions in silicon," *Nucl. Instrum. Methods Phys. Res. B, Beam Interact. Mater. At.*, vol. 287, pp. 124–129, Sep. 2012.

[30] Q. Gibaru, C. Inguimbert, P. Caron, M. Raine, D. Lambert, and J. Puech, "Geant4 physics processes for microdosimetry and secondary electron emission simulation: Extension of MicroElec to very low energies and 11 materials (C, Al, Si, Ti, Ni, Cu, Ge, Ag, W, Kapton and SiO_2)," *Nucl. Instrum. Methods Phys. Res. B, Beam Interact. Mater. At.*, vol. 487, pp. 66–77, Jan. 2021.

[31] S. Rocheman *et al.*, "Neutron induced energy deposition in a silicon diode," *IEEE Trans. Nucl. Sci.*, vol. 55, no. 6, pp. 3146–3150, Dec. 2008.

[32] P. Truscott, C. Dyer, A. Frydland, A. Hands, S. Clucas, and K. Hunter, "Neutron energy-deposition spectra measurements, and comparisons with Geant4 predictions," in *Proc. 8th Eur. Conf. Radiat. Effects Compon. Syst.*, Sep. 2005, pp. 1–6.

[33] B. Bergmann, S. Pospisil, I. Caicedo, J. Kierstead, H. Takai, and E. Frojdh, "Ionizing energy depositions after fast neutron interactions in silicon," *IEEE Trans. Nucl. Sci.*, vol. 63, no. 4, pp. 2372–2378, Aug. 2016.

[34] F. H. Ruddy *et al.*, "The fast neutron response of 4H silicon carbide semiconductor radiation detectors," *IEEE Trans. Nuclear Sci.*, vol. 53, no. 3, pp. 1666–1670, Jun. 2006.